Journal of Solid State Chemistry 182 (2009) 657–668

Contents lists available at ScienceDirect

Journal of Solid State Chemistry

journal homepage: www.elsevier.com/locate/jssc

Synthesis, crystal structure and photoluminescent properties of four lanthanide 5-nitroisophthalate coordination polymers

Yan Huang [a], Bing Yan [a,c,*], Min Shao [b]

[a] Department of Chemistry, Tongji University, Shanghai 200092, China
[b] Department of Chemistry, College of Science, Shanghai University, Shanghai 200444, China
[c] State Key Lab of Coordination Chemistry, Nanjing University, Nanjing 210093, PR China

ARTICLE INFO

Article history:
Received 24 June 2008
Received in revised form
17 November 2008
Accepted 24 November 2008
Available online 11 December 2008

Keywords:
Lanthanide
Coordination polymers
5-nitroisophthalic acid
Photoluminescence

ABSTRACT

Four new lanthanide coordination polymers, $[Y(Hnip)(nip)(H_2O)]\cdot H_2O$ (**1**), $[Ln(Hnip)(nip)(H_2O)_2]\cdot 2H_2O$ [*Ln* = Eu(**2**), Tb(**3**)] and $[Y(nip)_2]\cdot(H_2$4,4′-bpy$)_{0.5}$ (**4**) [5-nip = 5-nitroisophthalate, 4,4′-bpy = 4,4′-bipyridine], have been hydrothermally synthesized and structurally characterized. Compound **1** features novel lanthanide–carboxylate groups chains composed of three samehanded helical strands intersecting each other through hinged lanthanide atoms, and these chains are cross-linked by phenylene moieties of carboxylate ligands into a 2D layer structure. Compounds **2** and **3** are isomorphous, and contain 1D catenanelike *Ln*–O–C–O–*Ln* chains, which are interconnected by phenylene moieties into 2D layer structures. Compound **4**, however, displays a 3D architecture sustained by strong hydrogen bonding interactions between the protonated 4,4′-bpy and the carboxyl oxygen atom from $[Y_2(nip)_4]^{2-}$ with 2D layer structure, and 4,4′-bpy as the guest molecules exist in bilayer channel. The studies for the thermal stabilities of the four compounds show that compound **4** is more stable than other compounds. Compound **2** emits characteristic red luminescence of Eu^{3+} ions at room temperature, and its luminescent lifetime and quantum efficiency has been determined.

1. Introduction

The design and construction of architectures with fantastic topologies have been attracting considerable attention in supramolecular chemistry and crystal engineering in recent years [1–4]. Among them, the use of metal ions as nodes and bridging ligands as spacers has had a large impact on the building of coordination polymers with novel structures and is expected to lead to the development of exploitable properties such as magnetism, molecular sensors, luminescent materials, absorption materials, and so on [5]. Although many complexes have been well documented as 1D chains [6] and ladders [7], 2D grids [8], 3D frameworks [9], and helical staircase networks [10,11] in previous studies, the rational design of specific complexes with the above-mentioned properties is still a challenge for chemists.

In the design and assembly of the expected complexes, the selection of organic compounds as ligands is a key point. And rigid polycarboxylic acids, especially aromatic dicarboxylic acids such as phthalic, isophthalic and tertphthalic, are favorable ones for the researchers because of the flexible coordination modes and sensitivity to pH values of carboxylate groups, and the special system of rigid aromatic spacer that can have interesting electronic and magnetic interactions between the metal ions in the network through possible conjugative interaction [12]. Among these isomeric forms, the *m*-phthalate ligand usually acts as multi-dentate bridging ligand for its rich coordination modes. Furthermore, it is of interest to combine two or more different functionalities in a single polytypic ligand for the construction of coordination networks, with the expectation that incorporation of new properties with novel structural features may result. The nitryl group ($-NO_2$) as an electron-withdrawing group coexisting in isophthalic acid cannot only act as a hydrogen bond acceptor, but can also take on some spatial effects in the formation of polymeric networks [13]. Many coordination polymers of transition metal and 5-nitroisophthalic acid have been prepared [14–16], while its lanthanide coordination polymers are scarce [17,18]. The unique nature of lanthanide ions, such as their large radius, high and variable coordination numbers and the existence of multi-single electrons, makes the assembly of lanthanide complexes with novel structures and specific properties a remarkable challenging field of research. However, the fascinating coordination geometry and the interesting structures along with the special properties of lanthanide polymeric complexes have attracted increasing interest of chemists, and many studies have been reported in the literature recently [19–27]. In addition,

* Corresponding author at: Department of Chemistry, Tongji University, Shanghai 200092, China. Fax: +81 21 65982287.
E-mail address: byan@tongji.edu.cn (B. Yan).

0022-4596/$ - see front matter © 2008 Elsevier Inc. All rights reserved.
doi:10.1016/j.jssc.2008.11.033

the N-containing heterocyclic ligands, such as imidazole [28,29] and 4,4′-bipyridine (4,4′-bpy) [30,31], are frequently chosen as auxiliary ligands in many synthetic systems, which can play an important role in the syntheses of coordination polymers with interesting structural topologies and special properties.

Based on the above points, we used lanthanide nitrate, 5-nitroisophthalic acid and imidazole or 4,4′-bipyridine as reactants, and obtained a series lanthanide 5-nitroisophthalate coordination polymers: $[Y(Hnip)(nip)(H_2O)]\cdot H_2O$ (**1**), $[Ln(Hnip)(nip)(H_2O)_2]\cdot 2H_2O$ [$Ln = Eu$(**2**), Tb(**3**)] and $[Y(nip)_2]\cdot(H_2$4,4′-bpy$)_{0.5}$ (**4**). Their thermal stabilities and photoluminescent properties were also investigated. The present report is concerned with the syntheses, crystal structures and characterizations of compounds **1**–**4**.

2. Experimental

2.1. Materials and general methods

$Ln(NO_3)_3\cdot 6H_2O$ (Ln = Y, Eu, Tb, Gd) were prepared by dissolving their respective oxides in concentrated nitric acid followed by drying. All the other chemicals were purchased commercially and used without further purification. Elemental analyses (C, H, N) were determined with an Elementar Cario EL elemental analyzer. IR spectra were recorded with a Nicolet Nexus 912 AO446 spectrophotometer (KBr pellet), 4000–400 cm^{-1} region. Thermogravimetric analyses (TGA) were performed on an STA 409PC instrument in an air atmosphere with a heating rate of 10 °C/min. The X-ray powder diffraction (XRPD) was recorded on a Rigaku D/Max-2500 diffractometer at 40 kV, 100 mA for a Cu-target tube and a graphite monochromator. The luminescence (excitation and emission) spectra for the solid sample were determined with a Perkin-Elmer LS-55 spectrophotometer, whose excitation and emission slit width were 10 and 5 nm, respectively. Luminescent lifetimes for hybrid materials were obtained with an Edinburgh Instruments FLS 920 phosphorimeter using a 450 W xenon lamp as excitation source (pulse width, 3 μs). The outer luminescent quantum efficiency for was determined using an integrating sphere (150 mm diameter, $BaSO_4$ coating) from Edinburgh FLS920 phosphorimeter.

2.2. Synthesis of $[Y(Hnip)(nip)(H_2O)]\cdot H_2O$ (1)

A mixture of $Y(NO_3)_3\cdot 6H_2O$ (0.114 g, 0.3 mmol), 5-nitroisophthalic acid (0.095 g, 0.45 mmol), imidazole (0.020 g, 0.3 mmol) and water (5 mL) was sealed in a 15 mL stainless steel reactor with a Teflon liner and heated at 170 °C for 72 h. Colorless block crystals of **1** were obtained and washed with water. (Yield: 52%). $C_{16}H_{11}YN_2O_{14}$ (544.18): calcd. C 35.28, H 2.02, N 5.14; found C 35.30, H 1.99, N 5.12. IR (KBr pellet): (cm^{-1}) 3408 m, 3169 m, 3091 m, 1726 m, 1704 m, 1626 s, 1600 s, 1573 s, 1552 s, 1534 s, 1456 s, 1395 s, 1352 s, 1274 m, 1234 m, 1182 m, 1091 m, 1056 w, 930 m, 826 w, 791 m, 734 s, 708 m, 630 w, 543 m, 447 w.

2.3. Synthesis of $[Eu(Hnip)(nip)(H_2O)_2]\cdot 2H_2O$ (2)

A mixture of $Eu(NO_3)_3\cdot 6H_2O$ (0.133 g, 0.3 mmol), 5-nitroisophthalic acid (0.095 g, 0.45 mmol), imidazole (0.020 g, 0.3 mmol) and water (5 mL) was sealed in a 15 mL stainless steel reactor with a Teflon liner and heated at 170 °C for 72 h. Colorless block crystals of **2** were obtained and washed with water. (Yield: 50%). $C_{16}H_{15}EuN_2O_{16}$ (643.26): calcd. C 29.85, H 2.33, N 4.35; found C 29.90, H 2.30, N 4.33. IR (KBr pellet): $\tilde{\nu}$ = 3421 s, 3082 w, 1696 w, 1626 s, 1600 s, 1556 s, 1460 s, 1395 s, 1352 s, 1274 m, 1187 w, 1091 w, 930 w, 804 w, 787 w, 734 s, 691 w, 535 m.

2.4. Synthesis of $[Tb(Hnip)(nip)(H_2O)_2]\cdot 2H_2O$ (3)

A mixture of $Tb(NO_3)_3\cdot 6H_2O$ (0.136 g, 0.3 mmol), 5-nitroisophthalic acid (0.095 g, 0.45 mmol), imidazole (0.020 g, 0.3 mmol) and water (5 mL) was sealed in a 15 mL stainless steel reactor with a Teflon liner and heated at 170 °C for 72 h. Colorless block crystals of **3** were obtained and washed with water. (Yield: 51%). $C_{16}H_{15}TbN_2O_{16}$ (650.22): calcd. C 29.53, H 2.31, N 4.31; found C 29.50, H 2.33, N 4.30. IR (KBr pellet): $\tilde{\nu}$ = 3421 s, 3082 m, 1695 w, 1626 s, 1600 s, 1556 s, 1460 s, 1395 s, 1352 s, 1274 w, 1187 w, 1091 w, 930 w, 787 w, 734 s, 609 w, 535 m.

2.5. Synthesis of $[Y(nip)_2]\cdot(H_2$4,4′-bpy$)_{0.5}$ (4)

A mixture of $Y(NO_3)_3\cdot 6H_2O$ (0.114 g, 0.3 mmol), 5-nitroisophthalic acid (0.095 g, 0.45 mmol), 4,4′-bpy (0.047 g, 0.3 mmol), NaOH (0.018 g, 0.45 mmol) and water (5 mL) was sealed in a 15 mL stainless steel reactor with a Teflon liner and heated at 170 °C for 72 h. Colorless block crystals of **4** were obtained and washed with water. (Yield: 60%). $C_{21}H_{11}Y\,N_3O_{12}$ (586.24): calcd. C 42.99, H 1.88, N 7.16; found C 43.02, H 1.86, N 7.14. IR (KBr pellet): $\tilde{\nu}$ = 3443 m, 3174 m, 3095 m, 1722 m, 1617 s, 1600 s, 1552 s, 1460 s, 1395 s, 1348 s, 1274 m, 1235 w, 1183 w, 1087 m, 930 m, 817 m, 791 m, 734 s, 713 s, 630 w, 595 m, 552 m, 448 w.

2.6. Synthesis of $[Gd(Hnip)(nip)(H_2O)_2]\cdot 2H_2O$ (5)

The synthetic procedure of compound **5** is essentially the same as that for compounds **2** and **3**, while $Gd(NO_3)_3\cdot 6H_2O$ (0.136 g, 0.3 mmol) was used. (Yield: 49%). $C_{16}H_{15}GdN_2O_{16}$ (648.54): calcd. C 29.60, H 2.31, N 4.32; found C 29.58, H 2.34, N 4.30. IR (KBr pellet)/cm^{-1}: 3421 s, 3082 m, 1695 w, 1626 s, 1600 s, 1556 s, 1460 s, 1395 s, 1352 s, 1274 w, 1187 w, 1091 w, 930 w, 801 w, 787 w, 734 s, 609 w, 535 m.

2.7. X-ray crystallographic studies

Single-crystal X-ray data of compounds **1**, **2**, **3** and **4** were collected on a Bruker SMART 1000 CCD diffractometer equipped with graphite monochromatized Mo$K\alpha$ radiation (λ = 0.71073 Å). Semiempirical absorption corrections were applied using the SADABS program. All calculations were carried out with use of SHELXS 97 and SHELXL 97 programs [32]. All structures were refined on F^2 by full-matrix least-squares methods. The crystallographic data and structural determination of compounds **1**–**4** are summarized in Table 1. Selected bond lengths and angles for the four compounds are listed in Table 2. CCDC-644528, CCDC-653117, CCDC-653118, CCDC-644529 for compounds **1**, **2**, **3** and **4**, respectively, contain the supplementary crystallographic data for this paper. These data can be obtained free of charge from The Cambridge Crystallographic Data Center via www.ccdc.cam.ac.uk/data_request/cif.

3. Results and discussion

3.1. Syntheses

The syntheses of compounds **1**–**4** reported here were simply synthesized by mixing corresponding lanthanide nitrate with 5-nip ligand and the auxiliary imidazole ligand or 4,4′-bipyridine ligand in the molar ratio of 1:1.5:1 under hydrothermal reaction

Table 1
Crystal data and structure determination summary for compounds **1**–**4**.

Compound	1	2	3	4
Formula	$C_{16}H_{11}N_2O_{14}Y$	$C_{16}H_{15}N_2O_{16}Eu$	$C_{16}H_{15}N_2O_{16}Tb$	$C_{21}H_{11}N_3O_{12}Y$
M_n	544.18	643.26	650.22	586.24
T (K)	293(2)	273(2)	273(2)	273(2)
Crystal system	Monoclinic	Triclinic	Triclinic	Triclinic
Space group	$P2(1)/n$	P-1	P-1	P-1
a (Å)	13.9587(15)	9.6860(6)	9.6561(14)	8.6861(10)
b (Å)	8.7386(9)	10.5102(7)	10.4608(12)	9.3756(15)
c (Å)	16.6299(18)	13.5884(8)	13.5963(14)	13.8320(15)
α (°)	90	67.7540(10)	67.4990(10)	84.9700(10)
β (°)	106.4220(10)	69.9160(10)	69.7850(10)	77.8850(10)
γ (°)	90	65.0680(10)	65.0350(10)	73.8590(10)
V (Å^3)	1945.8(4)	1132.86(12)	1122.2(2)	1057.4(2)
Z	4	2	2	2
$D_{calcd.}$ (g/cm^3)	1.858	1.886	1.924	1.841
Absorption coefficient (mm^{-1})	3.081	2.852	3.235	2.837
F(000)	1088	632	636	586
Crystal size (mm)	0.30 × 0.20 × 0.20	0.30 × 0.20 × 0.20	0.30 × 0.25 × 0.25	0.30 × 0.20 × 0.20
θ range for data collection (°)	2.25–25.00	2.22–25.05	2.24–25.05	2.49–25.00
Reflections collected	9713	5890	5886	5529
Data ($I>2\sigma(I)$)/parameters	3426/308	3925/317	3907/317	3664/335
Goodness-of-fit on F^2	1.034	1.036	1.039	1.029
R_1 indices ($I>2\sigma(I)$)	0.0392	0.0192	0.0240	0.0323
wR_2 indices (all data)	0.1051	0.0452	0.0532	0.0769
Largest diff. peak/hole (e/Å^3)	1.530/−0.817	0.392/−0.474	0.544/−0.738	0.752/−0.409

Table 2
Selected bond distances (Å) and bond angles (°) for compounds **1**–**4**[a].

Compound 1			
Y–O1	2.244(3)	Y–O2A	2.360(3)
Y–O7	2.234(3)	Y–O8A	2.265(3)
Y–O9C	2.390(3)	Y–O10B	2.382(3)
Y–O10C	2.878(3)	Y–OW1	2.369(4)
O1–Y–O2A	146.78(11)	O7–Y–O8A	165.67(10)
O9C–Y–O10C	48.28(9)		
Compound 2			
Eu–O1	2.514(2)	Eu–O2	2.485(2)
Eu–O7	2.4063(19)	Eu–O8B	2.359(2)
Eu–O9C	2.377(2)	Eu–O10A	2.2974(19)
Eu–OW1	2.435(2)	Eu–OW2	2.442(2)
O2–Eu–O1	52.20(7)	O8B–Eu–O7	106.76(7)
O10A–Eu–O9C	102.63(7)		
Compound 3			
Tb–O1	2.352(3)	Tb–O2A	2.268(2)
Tb–O3C	2.373(2)	Tb–O4B	2.320(3)
Tb–O7	2.487(3)	Tb–O8	2.465(3)
Tb–OW1	2.399(3)	Tb–OW2	2.419(3)
O2A–Tb–O1	103.15(9)	O4B–Tb–O3C	105.48(9)
O8–Tb–O7	52.75(8)		
Compound 4			
Y–O1	2.250(2)	Y–O2A	2.249(2)
Y–O3D	2.417(2)	Y–O4D	2.381(2)
Y–O7	2.363(2)	Y–O8C	2.279(2)
Y–O9B	2.259(2)		
O2A–Y–O1	84.98(8)	O4D–Y–O3D	54.33(7)
O8C–Y–O7	94.99(8)		

[a] Symmetry codes **1**: A: $-x+3/2, y-1/2, -z+1/2$; B: $-x+2, -y+1, -z+1$; C: $x-1/2, -y+3/2, z-1/2$; D: $x+1/2, -y+3/2, z+1/2$; E: $-x+3/2, y+1/2, -z+1/2$. **2**: A: $x-1, y+1, z$; B: $-x+1, -y+2, -z$; C: $-x+1, -y+1, -z$; D: $x+1, y-1, z$. **3**: A: $-x+1, -y+1, -z+1$; B: $x, y-1, z$, C: $-x, -y+2, -z+1$; D: $x, y+1, z$. **4**: A: $-x, -y+2, -z+1$; B: $x-1, y, z$; C: $-x+1, -y+2, -z+1$; D: $-x+1, -y+1, -z+1$; E: $-x+2, -y, -z$; F: $x+1, y, z$.

conditions. Although imidazole does not exist in compounds **1**, **2** and **3**, it is necessary for the formation of compounds **1**, **2** and **3**. Experiments without imidazole ligand gave rise to clear solution and experiments with NaOH instead of imidazole ligand led to uncharacterized precipitates, which suggests that the existence of imidazole ligand may be helpful to the deprotonation of 5-H_2nip ligand and then the growth of compounds **1**, **2** and **3**, although the reactive mechanism, especially in hydrothermal or solvothermal conditions, was not clear.

3.2. Structural descriptions

An atom numbering diagram of the fundamental unit of **1** is shown in Fig. 1. Compound **1** crystallizes in the monoclinic system, space group $P2_1/n$. There is only one crystallographically independent yttrium ion in the structure. The local coordination geometry for the eight-coordinate Y(III) is close to a trigonal dodecahedron coordinated by one pair of oxygen atoms from a 5-nip^{2-} anion, three bridging oxygen atoms from three 5-nip^{2-} anions, two bridging oxygen atoms from two 5-Hnip$^-$ anions, and one oxygen atom from one terminal water molecule. The Y–O (carboxylate) bond distances range from 2.234(3) to 2.878(3) Å, and that of Y–O (aqua) is 2.369(4) Å. The bond angles consisting of yttrium ions and the carboxylate oxygen atoms are 146.78(11)° (O1–Y–O2A), 165.67(10)° (O7–Y–O8A) and 48.28(9)° (O9C–Y–O10C), respectively.

Two kinds of anions for 5-H_2nip, 5-Hnip$^-$ and 5-nip^{2-} exist in the asymmetric unit, and their coordination modes are shown in Scheme 1a and b. The 5-Hnip$^-$ ligand adopts a bidentate coordination mode (Scheme 1a) and bridges adjacent Y(III) ions to form a helical-shape chain along b-axis (Fig. 2). Along the chain, the Y1⋯Y1A distance is 4.6103(7) Å and the Y1*–Y1–Y1* angle is 142.782(10)°. Each 5-nip^{2-} ligand acts as a pentadentate ligand with one bidentate carboxylate group and one μ_2-η^2:η^1 carboxylate group (Scheme 1b), and the two types of carboxylate groups bridge adjacent Y(III) ions into another two kinds of helical-shape chains. Unexpectedly, the three kinds of helical-shape chains are the samehanded helical strands with a pitch of 8.878(6) Å and intersect each other through hinged Y atoms, thus forming a unique yttrium–carboxylate groups chain. This is, to our knowledge, the first example of lanthanide–carboxylate groups chain entwined by triple helical strands. These chains are further cross-linked by the phenylene moieties of the 5-nip^{2-} ligands to yield

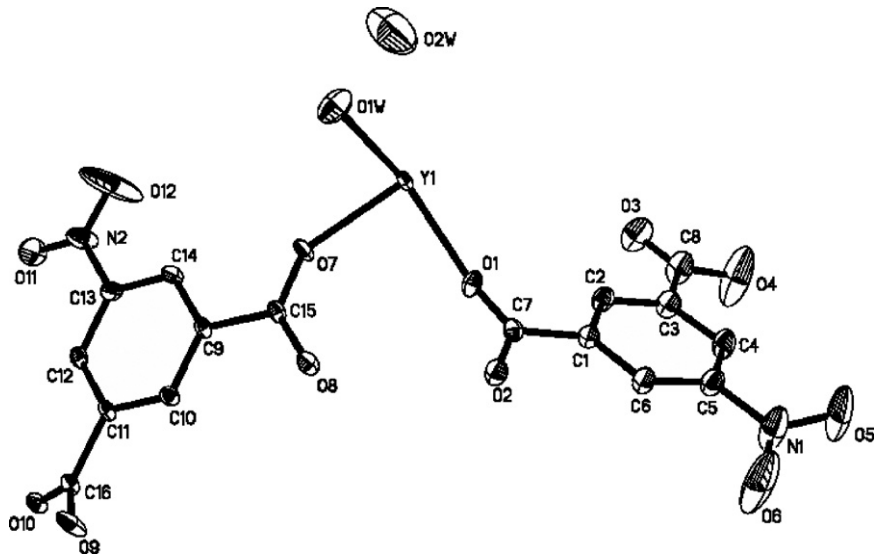

Fig. 1. Coordination environment of Y(III) ion with atom labeling in 1. Hydrogen atoms are omitted for clarity.

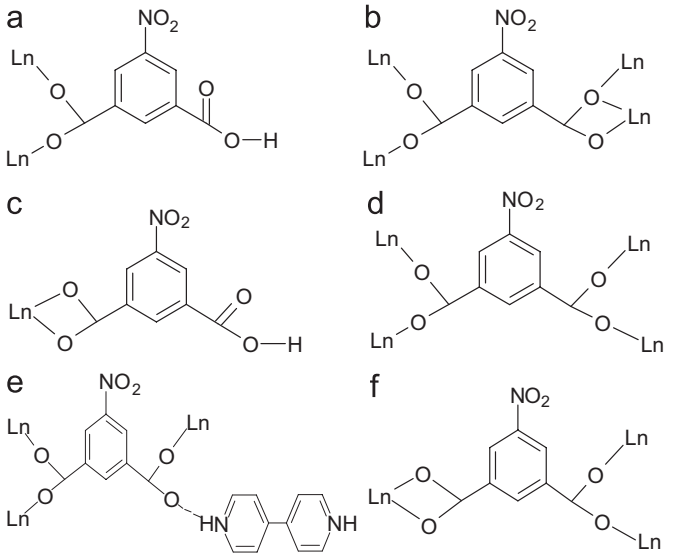

Scheme 1. Coordination modes of 5-nitroisophthalic acid observed in compounds 1–4. (a) Bridge coordination mode; (b) chelating-bridging pentadentate coordination mode; (c) chelate coordination mode; (d) bridging-bridging tetradentate coordination mode; (e) bridging-monodentate coordination mode; (f) chelating-bridging tetradentate coordination mode.

the final 2D layers (Fig. 3b and c). The lattice water molecules are located between the 2D layers, forming a number of hydrogen bonds with nitryl oxygen atoms, carboxylate oxygen atoms of nip^{2-} anions and coordinated water molecules (O···O = 2.809(7)–3.501(7) Å). The uncoordinated carboxyl oxygen atoms of 5-$Hnip^{-}$ anions are also involved in hydrogen bonding with the coordinated water molecules at a distance of 3.080(7) Å. Moreover, due to the spatial effect of the nitryl group (–NO_2), the intra-layer 5-nip^{2-} and inter-layer 5-$Hnip^{-}$ are all antiparallelly arranged, which may facilitate anti-parallel slipped π–π stacking. The inter-layer anti-parallel 5-$Hnip^{-}$ aromatic rings present average centroid–centroid distance and interplanar distance of 3.747(9) and 3.575(7) Å with an offset angle of 17.44°, and the intra-layer anti-parallel 5-nip^{2-} aromatic rings present average centroid-centroid distance and interplanar distance of 3.675(1) and 3.348(9) Å with an offset angle of 24.32°, indicating the existence of π–π interactions, stabilizing the 3D supramolecular structure (Fig. 4).

Results of single crystal X-ray diffraction show that the crystal structures of compounds **2** and **3** are isomorphous, so compound **2** is chosen as a representative. An atom numbering diagram of the fundamental unit for compound **2** is shown in Fig. 5. Similar to the allomer of Sm, Gd and Dy complexes [17], compound **2** crystallizes in the triclinic system, space group *P*-1. The coordination geometry of the Eu(III) ion is close to a bicapped trigonal prism coordinated by one pair of chelating oxygen atoms from one 5-$Hnip^{-}$ anion, four bridging oxygen atoms from four 5-nip^{2-} anions and two oxygen atoms from two terminal water molecules. The Eu–O (carboxylate) bond distances range from 2.2974(19) to 2.514(2) Å, and those of the Eu–O (aqua) bonds are 2.435(2) and 2.442(2) Å. Compound **3** possesses the similar structure and the Tb–O bond lengths are in the range of 2.268(2)–2.487(3) Å.

There also exist two kinds of anions for H_2nip in one unit of compound **2**, and their coordination modes are shown in Scheme 1c and d. Differing from compound **1**, the carboxylate groups of nip^{2-} ligand adopt bridging-bridging coordination mode to connect Eu(III) ions into a 1D catenanelike Eu–O–C–O–Eu chain (Fig. 6), with the Eu···Eu distance of 4.786(8) and 5.012(1) Å, respectively. Adjacent chains are further cross-linked by the phenylene moieties of the 5-nip ligand to yield the final 2D layers (Fig. 7a and b), which are decorated with 5-$Hnip^{-}$ anions. In addition, the 2D layers are connected by rich hydrogen bonds to form a 3D supramolecular architecture (Fig. 1S, Supporting information), and the 3D supramolecular structures are further stabilized by π–π interactions between the intra-layer antiparallel nip^{2-} aromatic rings in an offset fashion with the interplanar distance of 3.423(9) Å, centroid-centroid distance of 3.5362 Å and an offset angle of 14.48°.

The framework of compound **4** crystallizes in the triclinic space group P-1 and consists of hydrogen-bonded two-dimensional bilayers as the fundamental building unit. As shown in Fig. 8, each Y(III) ion is coordinated by one pair of chelating oxygen atoms from one nip^{2-} anion and five bridging oxygen atoms from five nip^{2-} anions, showing an uncommon distorted single-cap triangular prism [18]. The Y–O bond distances range from 2.249(2) to 2.417(2) Å, which are within the normal ranges.

There is only one kind of anion for 5-H_2nip, 5-nip^{2-} in compound **4**, and the 5-nip^{2-} anions adopt two kinds of coordination modes as shown in Scheme 1e and f. The 5-nip^{2-}

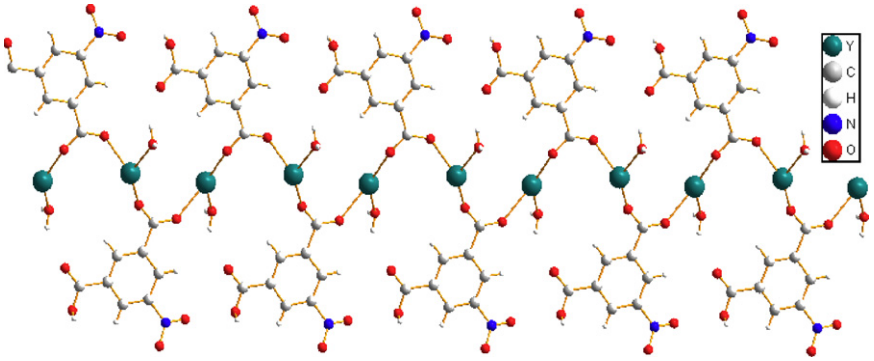

Fig. 2. The 1D helical chain formed by Y(III) ions and $Hnip^{-}$ ligands in compound 1.

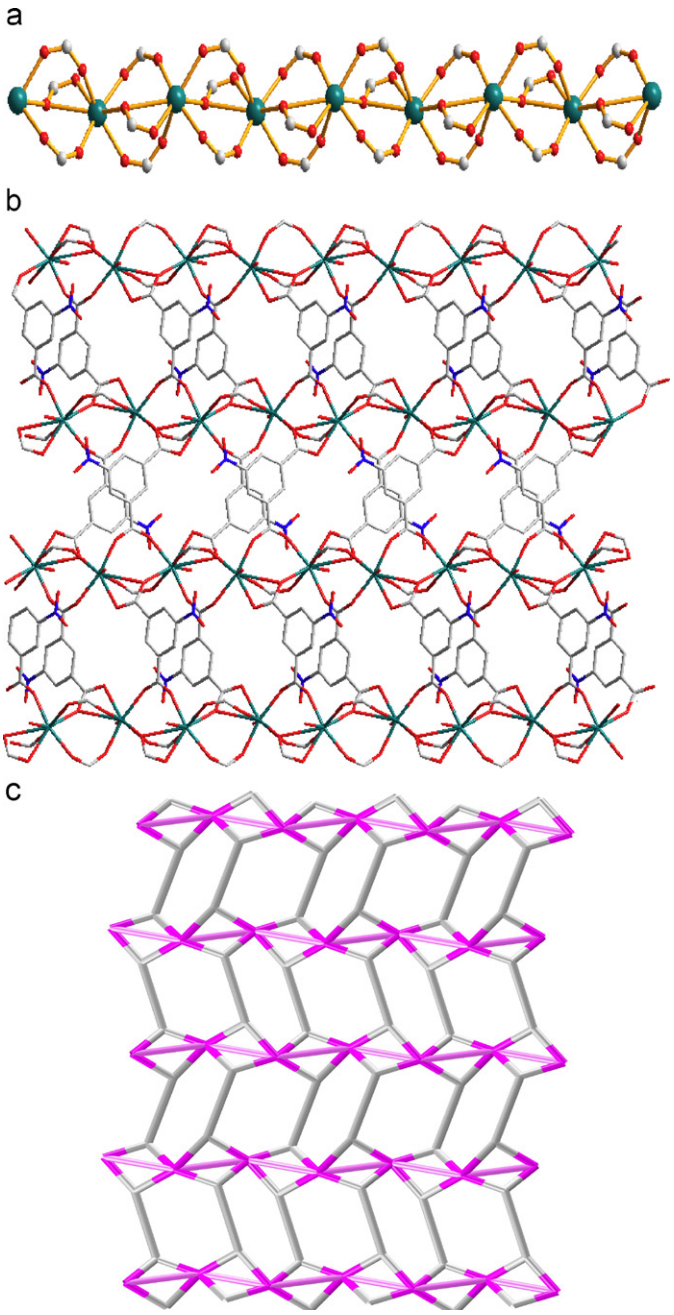

Fig. 3. (a) The 1D yttrium–carboxylate groups chain entwined by triple helical chains in compound 1. (b) The 2D layer structure of compound 1. (c) A simplified 2D network perspective view of 1. Hydrogen atoms have been omitted for clarity.

anion of the first type adopts bridging-monodentate mode (Scheme 1e) to coordinate with Y ions, forming a 1D chain along the *a*-axis (Fig. 9). Along the chain, the Y···Y distances are 4.5367(7) and 5.5196(7) Å, and the Y1*–Y1–Y1* angle is 119.156(8)°. In the 1D chain, there are two types of chair-shaped rings: one is an eight-member ring composed of two Y(III) ions and two carboxylate groups, and the other is a 16-member ring formed by two 5-nip^{2-} ligands bridging two Y(III) ions. The 5-nip^{2-} ligand of the other type acts as a tetradentate ligand (Scheme 1f) with one chelate carboxylate group and two bridging carboxylate group, which join the 1D chains and construct another kind of 1D Y–O–C–O–Y chains (Fig. 2S, Supporting information). Adjacent 1D Y–O–C–O–Y chains are further cross-linked by the phenylene moieties of the 5-nitroisophthalate ligands to yield the final 2D layers (Fig. 10b and c).

To balance the charge, we consider the 4,4′-bpy molecules to be protonated, which are not engaged in coordinating with the metal ion, and exist in the gaps between layers as guest molecules [18]. The nitrogen atom N3 from the protonated 4,4′-bpy molecules and the carboxyl oxygen atoms O10 form a strong hydrogen bond (N3-O10G distance: 2.541(3) Å, symmetry codes: #7 $x-1, y-1, z$). The hydrogen bonds join two adjacent sheets, by which the 2D structure packs into a 3D structure (Fig. 3S, Supporting information). Also, the 3D structures are further stabilized by π–π interactions between the intra-layer antiparallel nip^{2-} aromatic rings in an off-set fashion with the interplanar distance of 3.3382 Å, centroid-centroid distance of 3.8250 Å and an offset angle of 29.22°. Comparing the structure of compound **4** with that of compound **1**, it is not difficult to find that the presence of 4,4′-bpy molecules lead to the decreased coordination number of central Y(III) ion and different coordination modes of carboxylate ligands although 4,4′-bpy molecules do not bond with central Y(III) ion, which leads to the distinct 3D architecture. Compound **4**, however, has the similar architecture with that of $[Er(nip)_2]\cdot(H_2$4,4′-bpy$)_{0.5}$ [18], which may be due to the similar radius of Y(III) and Er(III).

Davis and Lobo had addressed templating in zeolites in great detail [33], and their discussion can be further extended to templates in metal-organic framework (MOF) systems. In their definition, the organic guest molecules act in one of three roles as space-filling species, structure-directing agents, or true templates. In compound **4**, the guest molecules are clearly space-filling species and quite arguably structure-directing agents. By introducing the molecular species into the channels of compound **1**, compound **4** with distinct topology was obtained, supporting the role of the species as a structure-directing agent. Davis and Lobo had also asserted further that in true templating, free rotation of the guest molecule must not occur, as the molecule itself does not induce the topology of the overall structure but rather the volume needed to allow molecular rotation. The ordering and fixed

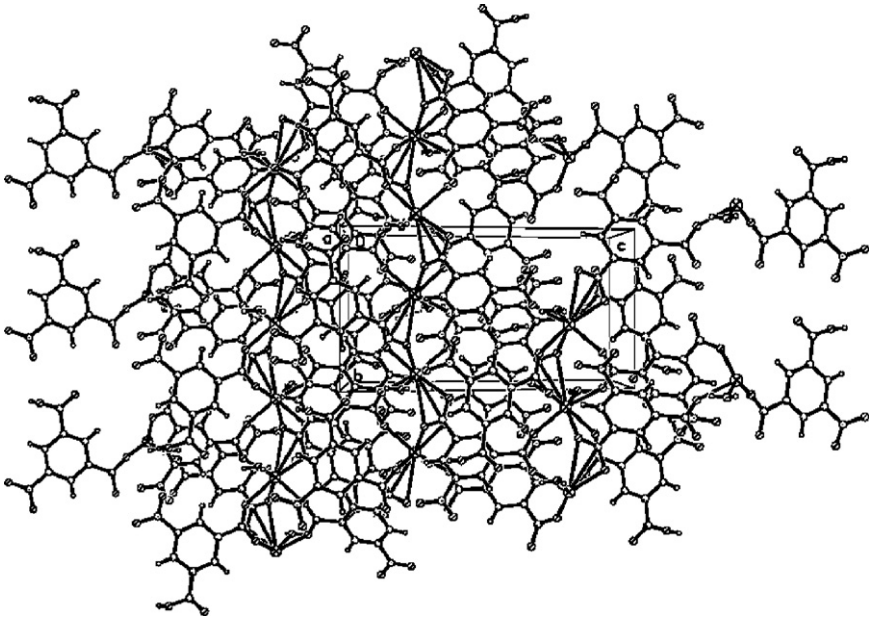

Fig. 4. The 3D supramolecular architecture of compound 1 viewed along *a*-axis. Dotted lines represent hydrogen bonding interaction.

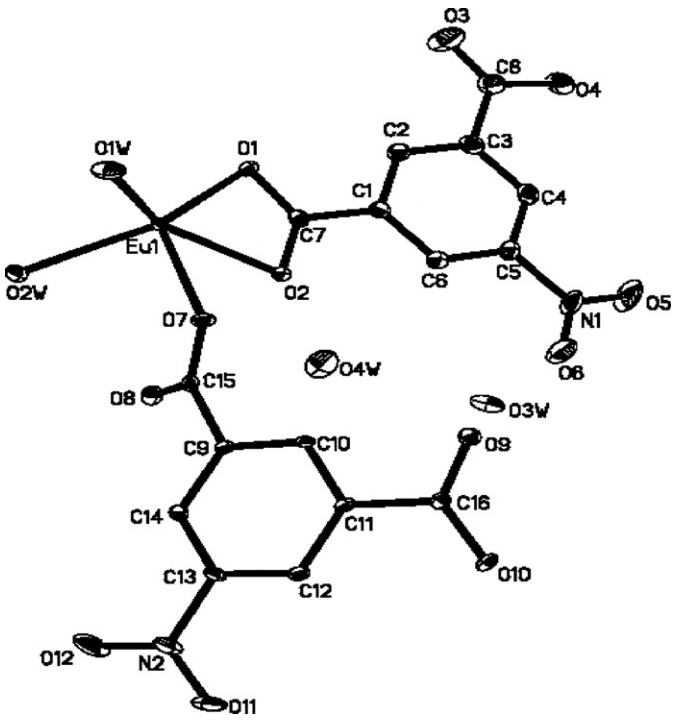

Fig. 5. Coordination environment of Eu(III) ion with atom labeling in 2. Hydrogen atoms are omitted for clarity.

positions of the 5-nip ligands and 4,4′-bpy molecules in compound **4** may in fact support a "true templating model" [30].

3.3. Thermogravimetric analysis

To investigate the thermal stability of the four compounds, TGA analyses have been carried out on crystalline sample with a NETZSCH STA 409PC unit, at a heating rate of 10 °C/min under an air atmosphere. As shown in Fig. 11, TGA curves of compound **1** exhibit two main steps of weight losses. The first step starts at 56 °C and completes at 259 °C, which corresponds to the release of aqua ligands and lattice water molecules. The observed weight loss of 6.86% is close to the calculated value (6.62%). The second weight loss region occurs over the range 259–700 °C and consists of three gradual losses. The total loss in this region has a magnitude of 75.21% and is accounted for by the complete decomposition of the $Hnip^-$ and nip^{2-} ligands (calculated mass loss 77.05%). Above 700 °C, the TGA curve does not change with the temperature, suggesting that a residue, Y_2O_3, has been obtained in 19.48% yield (calculate: 20.75%), supported by the powder XRD pattern (Fig. 4S(a), Supporting information). Compounds **2** and **3** are isostructural, and their TGA curves are similar. The weight losses of aqua ligands and lattice water molecules are both in the temperature range 50–250 °C for **2** and **3**, the complete decomposition of the $Hnip^-$ and nip^{2-} ligands is in the temperature range 290–770 and 290–650 °C for **2** and **3**, respectively, and then lanthanide oxide (the powder XRD patterns are shown in Fig. 4S((b) and (c)), Supporting information) is obtained in 25.65% yield (calculated: 27.36%) and 25.74% yield (calculated: 20.75%) for **2** and **3**, respectively. TGA of compound **4** shows that compound **4** remains stable up to 400 °C, at which temperature the decomposition of compound **4** begins and ends at 720 °C. This process is attributed to the loss of 4,4′-bpy and carboxylate ligands with a weight loss of 83.44% (calculated: 84.78%). Above 720 °C, the TGA curve does not change with the temperature, suggesting that a residue, Y_2O_3, has been obtained in 20.17% yield (calculated: 19.26%), proven by the powder XRD pattern (Fig. 4S(d), Supporting information). From the TGA curves of the four compounds, we can see that compound **4** is more stable than other compounds, which may be due to the different guest molecules filling between 2D layers, water in compounds 1–3 and 4,4′-bpy in compound **4** [18].

3.4. Photoluminescent properties

Compound **2** exhibits red photoluminescence of Eu^{3+} upon the radiation of UV light in the solid state at the room temperature (Fig. 12). As shown in Fig. 12(a), a broad excitation band ranging in 315–350 nm appears with maximum excitation peak of 324 nm, corresponding to the absorption of 5-H_2nip ligand, which will benefit the energy absorption and transfer to Eu^{3+}. Besides, two

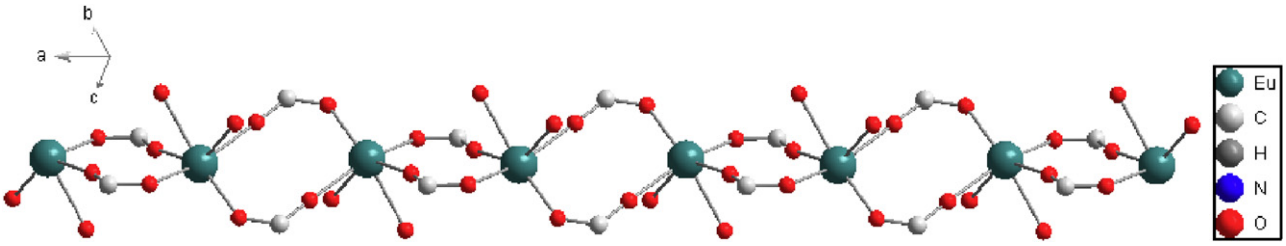

Fig. 6. View of 1D catenanelike Eu–O–C–O–Eu chain in 2. Hydrogen atoms are omitted for clarity.

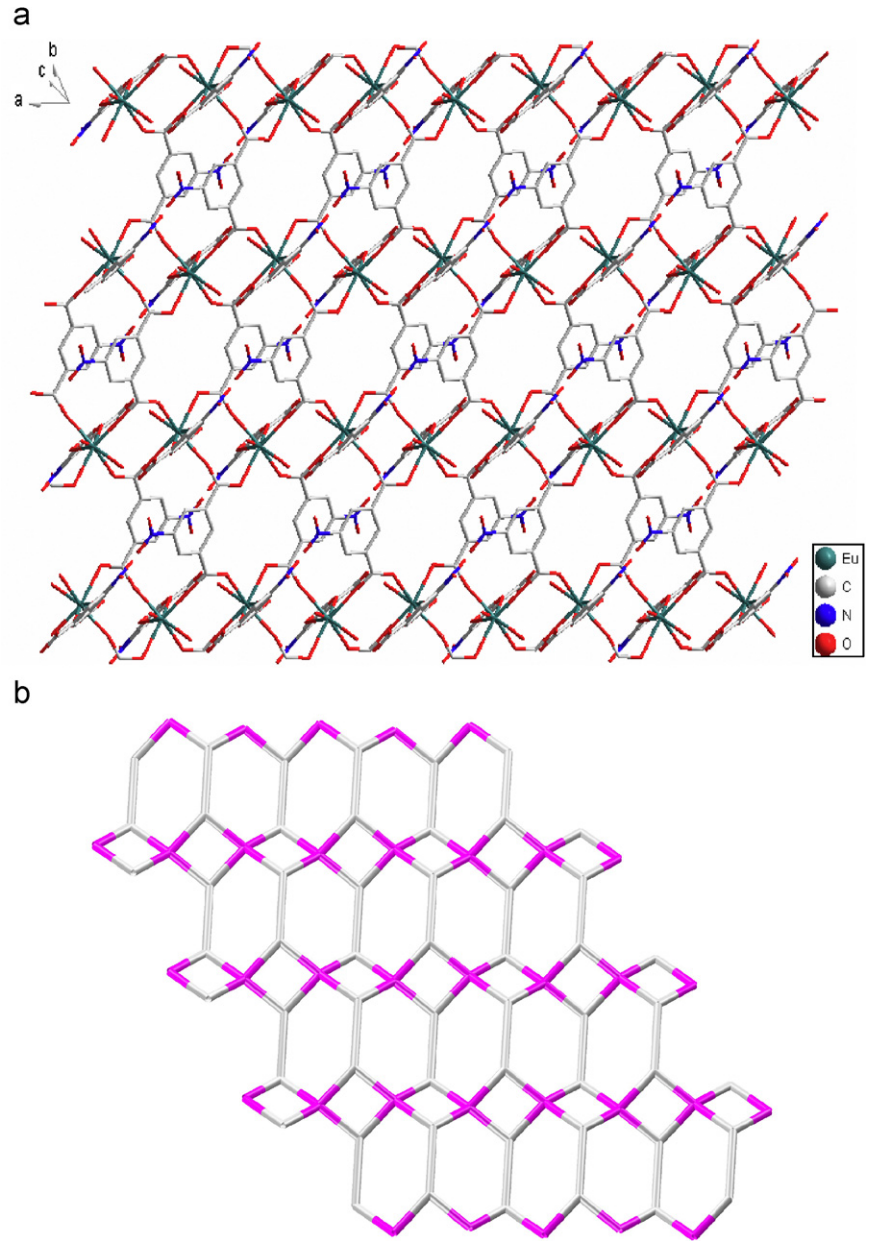

Fig. 7. (a) The 2D layer structure of compound 2. (b) A simplified 2D network perspective view of 2.

apparent sharp excitation bands can be observed in the range of 350–400 nm with peaks at 380 and 392 nm, which can be ascribed to the *f*–*f* transitions of Eu^{3+}. Under excitation at 392 nm, the emission spectra of compound **2** at room temperature (Fig. 12(b)) shows five emission bands: 576, 589, 611, 650 and 696 nm, which are attributed to be the characteristic emission $^5D_0 \rightarrow {}^7F_J$ ($J = 0$–4) transition of Eu(III), respectively. The narrow-band emission at 613 nm is characteristic of the hypersensitive $^5D_0 \rightarrow {}^7F_2$ transition of Eu(III), which is much more intense than the $^5D_0 \rightarrow {}^7F_1$ transition at 588 nm. This observation is consistent with the fact that the Eu centers in two do not possess inversion symmetry [34].

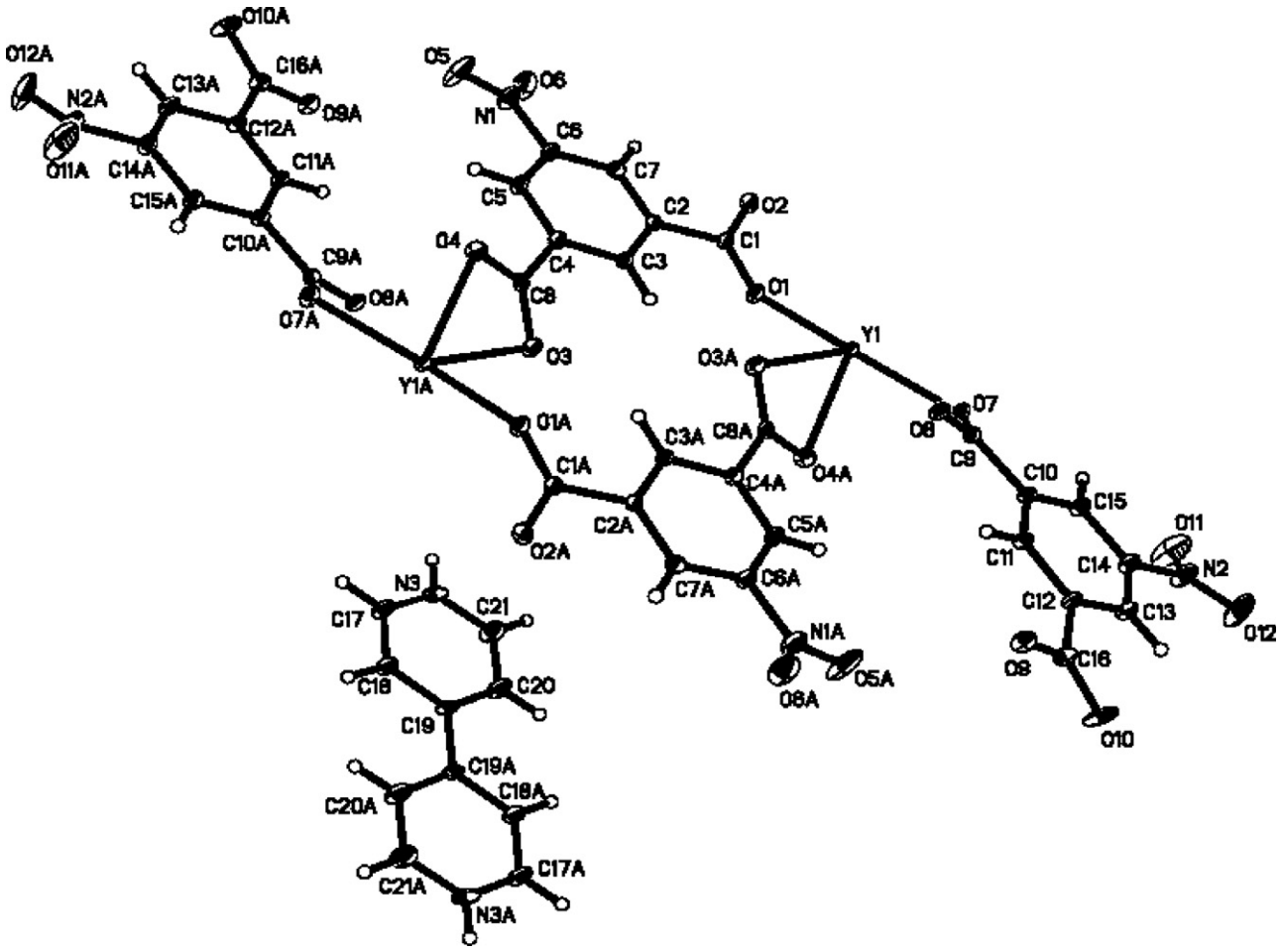

Fig. 8. Coordination environment of Y(III) ion with atom labeling in 4.

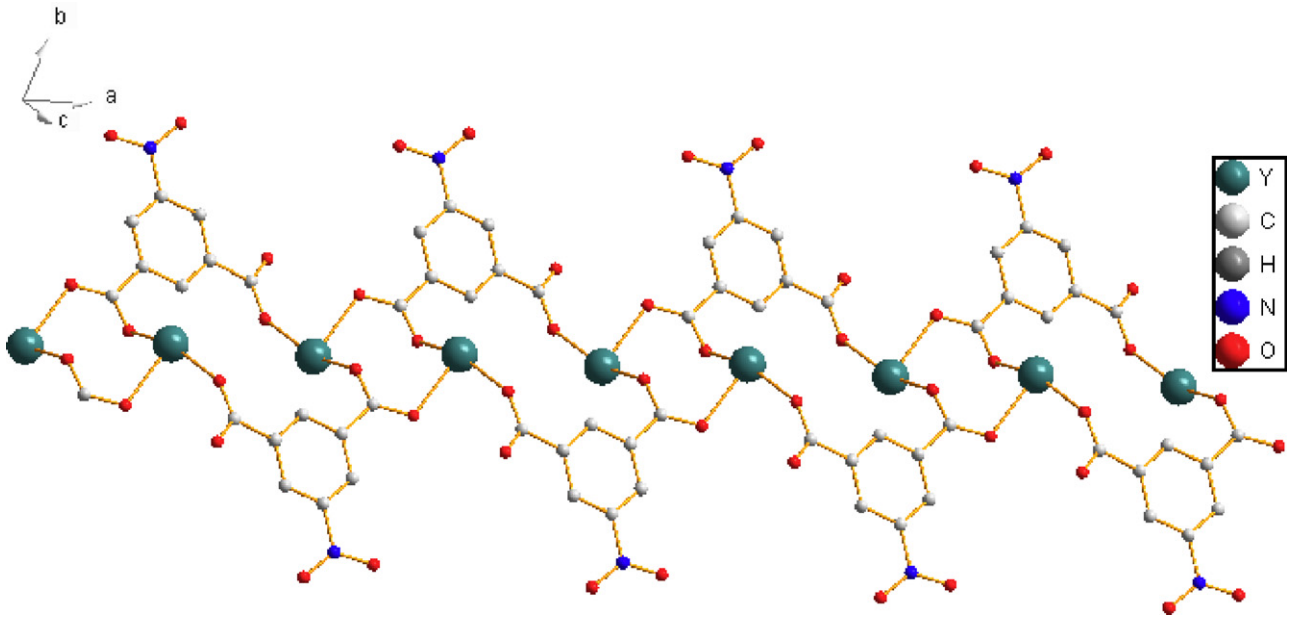

Fig. 9. The 1D chain formed by Y(III) ions and nip^{2-} ligands with bridging-monodentate coordination mode in compound 4.

However, we cannot observe the characteristic emission of Tb^{3+} of compound **3** under the radiation of UV light at the room temperature. It is well known that the luminescence of lanthanide complexes upon excitation into the ligand absorption band arises from *f–f* transitions from the radiative level of *Ln*(III) to their lower-lying states. It should be emphasized that transitions

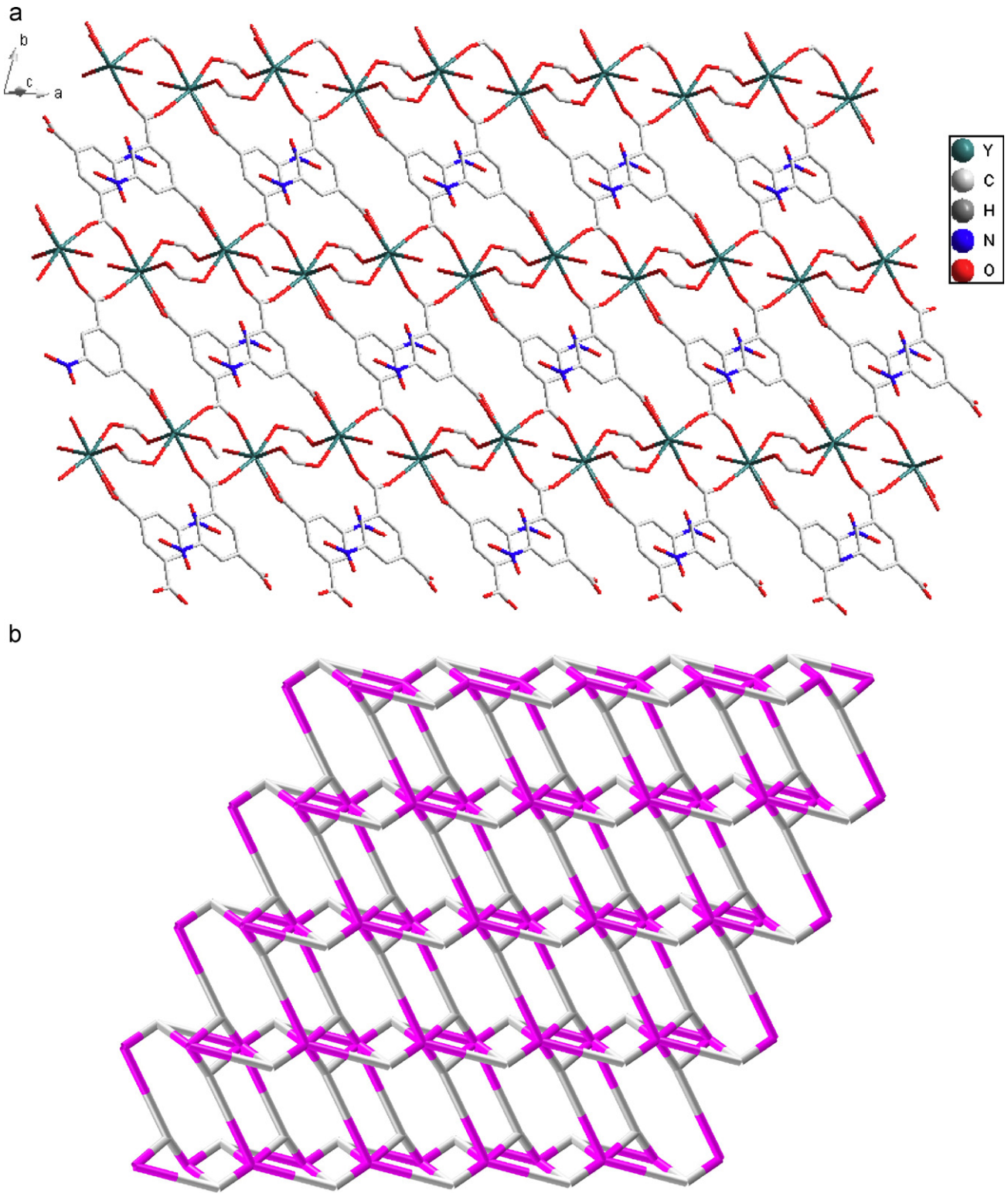

Fig. 10. (a) The 2D layer structure formed by Y(III) ions and nip^{2-} ligands. (b) A simiplied 2D network perspective view of 4. The benzene rings of nip^{2-} ligands with bridging-monodentate coordination mode have been omitted for clarity.

between the f-states are formally parity-forbidden (Laporte's rule), which, in turn, results in long radiative lifetimes (up to the millisecond timescale) and line-like emission bands [35,36]. The excited levels of *Ln*(III) ions are usually populated as a result of energy transfer from the triplet level of the organic ligand, which is formed by rapid intersystem crossing. So, the energy of the triplet states of coordinated ligands plays an important role in the efficiency of the energy transfer: they should lie close to the resonant levels of the lanthanide ion but sufficiently high to prevent back energy-transfer [37]. In order to determine the triplet energy levels of rare earth complexes, it is common practice to use analogous complexes of a nonemitting lanthanide

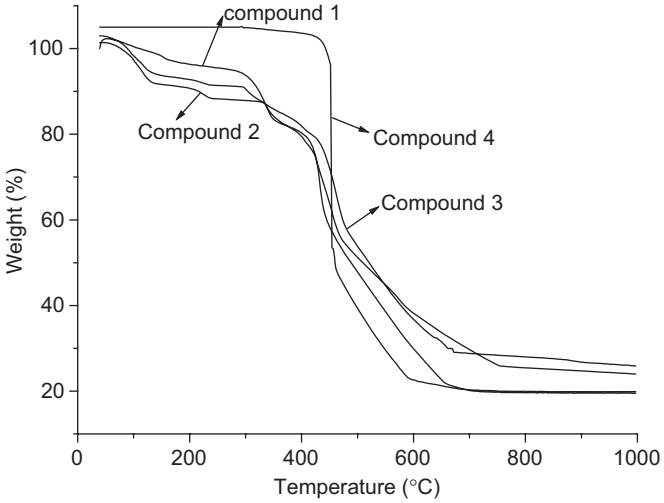

Fig. 11. The TGA curves of compounds 1–4.

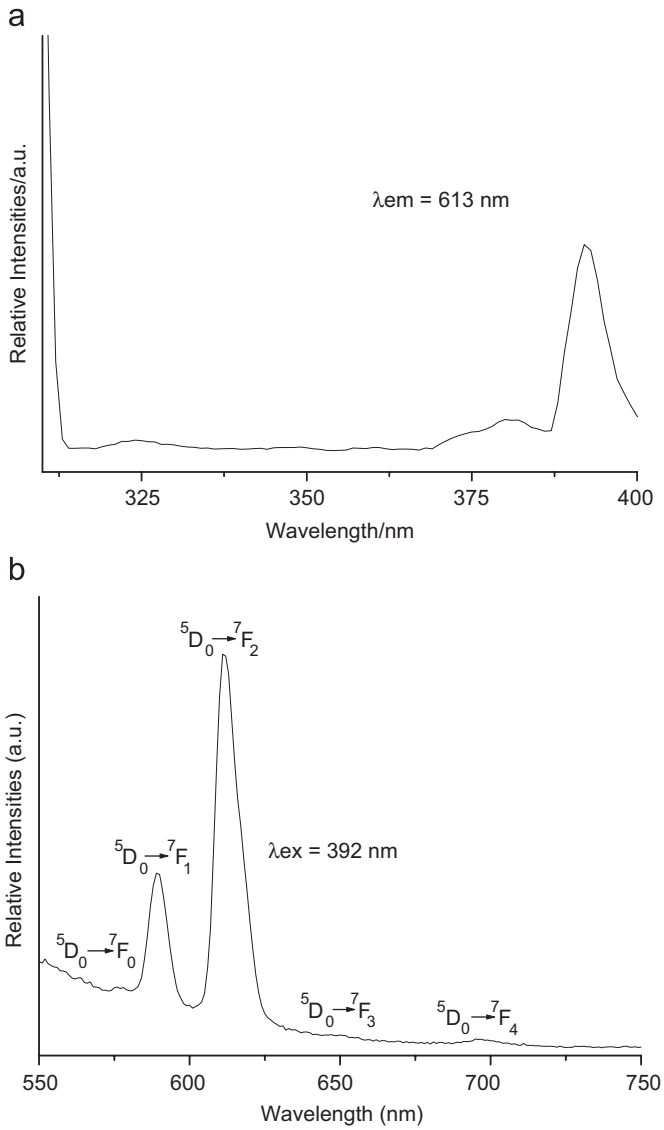

Fig. 12. The photoluminescence spectrum of compound 2: (a) the excitation spectrum of compound 2 at 613 nm and (b) the emission spectrum of compound 2 at 392 nm.

Table 3
The lowest triplet energy of Gd^{3+} complex with 5-H_2nip and the energy difference.

Lanthanide	Lowest triplet state energy of 5-H_2nip (Tr, cm^{-1})	The lowest excited level of Ln^{3+} (Ln^{3+}, cm^{-1})	ΔE(Tr–Ln^{3+}) (cm^{-1})
Eu	21786	17331	4455
Tb	21786	20500	1286

Ln^{3+}: Eu^{3+}, $^5D_0$ (17331 cm^{-1}); Tb^{3+}, $^5D_4$ (20500 cm^{-1}).

ion (i.e., La^{3+}, Gd^{3+}, and Lu^{3+}). In the case of Gd^{3+}, the emitting energy level of this ion (~32000 cm^{-1}) is so much higher than the triplet state of organic ligands that energy transfer is not possible. The organic triplet state will thus deactivate through radiative transition to the ground-state resulting in molecular phosphorescence. With the absence of the lanthanide characteristic *f–f* emission, the emission spectra of the Gd^{3+} complexes exhibit only the phosphorescence bands corresponding to the ligand-centered triplet energy levels. Since the energy of the ligand-centered triplet state does not depend significantly on the metal, we can use the Gd^{3+} analog of the complexes to measure the 0-0 transition and obtain the lowest triplet state energy of analogous Ln^{3+} complexes. For this reason, we have synthesized the Gd^{3+} analogs of the complexes under study [38]. The phosphorescence spectrum of the gadolinium complex was measured at 77 K in DMF solution (as shown in Fig. 5S, Supporting information). The gadolinium analog gave an emission at 459 nm (21786 cm^{-1}), and this was taken as the triplet state energy of 5-H_2nip. The energy differences between the triplet state of 5-H_2nip and the resonance energy level of Ln^{3+} (Ln = Eu, Tb) were calculated, the data are shown in Table 3.

In addition, according to Sato's result [39], the intramolecular energy migration efficiency from organic ligands to the central Ln^{3+} is the most important factor influencing the luminescence properties of rare earth complexes. The intramolecular energy transfer efficiency depends mainly on the two energy transfer processes [40]. One is from the lowest triplet state energy of organic ligands to the resonant energy level by Dexter's resonant exchange interaction theory [41]: with the decrease in the energy difference between the triplet state energy of conjugated carboxylic acid and Ln^{3+}, the intramolecular energy rate constant is increased. The other is the inverse energy transition by the thermal deactivation mechanism [42]: the inverse energy transfer rate constant increases with decreasing ΔE(Tr–Ln^{3+}). As discussed above, there should exist an optimal energy difference between the triplet position of 5-H_2nip and the emissive energy level of Ln^{3+}, the larger and the smaller ΔE(Tr–Ln^{3+}) will decrease the luminescence properties of rare earth complexes [43,44]. In Table 3, the lowest triplet state energy of H_2nip is higher than the resonant energy level of Ln^{3+} (Ln = Eu, Tb) and the energy difference is 4455 cm^{-1} for $Eu^{3+}$and 1286 cm^{-1} for Tb^{3+}, respectively. And it may be deduce that the triplet state energy level of 5-H_2nip ligand matches better to the lowest resonance level of Eu^{3+} than Tb^{3+}; because such small ΔE(Tr–Tb^{3+}) could result in the non-radioactive deactivation of the terbium emitting state via a back-energy transfer process and might quench the luminescence of the Tb complex [45], we do not observe the luminescence of the Tb compound at room temperature in solid state or in solutions.

Further, the luminescence lifetime for $^5D_0 \rightarrow {}^7F_2$ emission (331 μs) was measured and the corresponding quantum efficiency for Eu^{3+}'s $^5D_0$ emission of compound 2 was then calculated. The typical decay curve of compound **2** can be described as a single exponential ($Ln(S(t)/S_0) = -k_1 t = -t/\tau$), indicating that Eu^{3+} ions occupy the same coordination environment. According to the four

main equations [46,47], the emission quantum efficiencies of the $^5D_0$ europium ion excited state for Eu^{3+} complex was selectively determined on the basis of the emission spectra and lifetimes of the $^5D_0$ emitting level.

$$A_{0J} = A_{01}(I_{0J}/I_{01})(\upsilon_{01}/\upsilon_{0J}) \quad (1)$$

$$A_{rad} = \Sigma A_{0J} = A_{00} + A_{01} + A_{02} + A_{03} + A_{04} \quad (2)$$

$$\tau = A_{rad}^{-1} + A_{nrad}^{-1} \quad (3)$$

$$\eta = A_{rad}/(A_{rad} + A_{nrad}) \quad (4)$$

Here A_{0J} is the experimental coefficients of spontaneous emissions, among A_{01} is the Einstein's coefficient of spontaneous emission between the $^5D_0$ and $^7F_1$ energy levels, which can be determined to be 50 s^{-1} approximately [46,47] and as a reference to calculate the value of other A_{0J}. I is the emission intensity and can be taken as the integrated intensity of the $^5D_0 \rightarrow {}^7F_J$ emission bands [46,47]. υ_{0J} refers to the energy barrier and can be determined from the emission bands of Eu^{3+}'s $^5D_0 \rightarrow {}^7F_J$ emission transitions. A_{rad} and A_{nrad} mean to the radiative transition rate and nonradiative transition rate, respectively, among A_{rad} can be determined from the summation of A_{0J} (Eq. (2)). And then the luminescence quantum efficiency (7.5%) can be calculated from the luminescent lifetimes, radiative and nonradiative transition rates. Further, we can select Hnip as the energy donor (whose luminescent quantum efficiency can be determined as 23.5%) and Eu^{3+} as the energy acceptor in the complex 2 system, then the energy transfer efficiency can be determined as 32% according to the method in Ref. [48]. The energy transfer from Hnip to Eu^{3+} is not large, which takes agreement with the luminescent behavior of complex 2. According to Horrocks' previous research [49], it is therefore expected that probable number of coordinated water molecules (n_w) can be calculated as following equations:

$$n_w = 1.05(A_{exp} - A_{rad}) \quad (5)$$

The coordinated water molecules can be estimated to be three and is different from the structure (2), whose distinction may be ascribed as the existence of two crystal water molecules. The much hydroxyl groups of water molecules produce the severe non-radiative transition to decrease the luminescent efficiency.

4. Conclusions

In summary, we have successfully synthesized four new lanthanide coordination polymers with 5-nitroisophthalic acid. In the four lanthanide coordination polymers, carboxylate ligands connect lanthanide ions into 2D layer structures, which are all constructed by phenylene moieties-connected *Ln*–O–C–O–*Ln* chains. These 2D layer structures are further extended into 3D supramolecular networks through hydrogen bonding interaction and π–π aromatic stacking interaction. Compound **4** demonstrates the effect a template has on overall framework structure and shows much higher thermal stability than other three compounds. The lowest triplet level of 5-H_2nip ligand was calculated from the phosphorescence spectrum of Gd–nip complex, and the energy transfer mechanisms in the lanthanide compounds were discussed. In isostructural compounds **2** and **3**, compound **2** emits characteristic red fluorescence of Eu^{3+} ion while compound **3** does not exhibit the characteristic emission of Tb^{3+} ion, which suggests that the different energy transfer processes take place. The results illustrate that the coordination preference of different lanthanide ions and the nature of ligands have a great influence on the structures and properties of the metal-organic compounds.

Acknowledgment

This work was financially supported by the National Natural Science Foundation of China (20671072).

Appendix A. Supporting information

Supplementary data associated with this article can be found in the online version at doi:10.1016/j.jssc.2008.11.033.

References

[1] P.J. Hagrman, D. Hagrman, J. Zubieta, Angew. Chem. Int. Ed. 38 (1999) 2638–2684.
[2] S.S. Chui, S.M.F. Lo, J.P.H. Charmant, A.G. Orpen, I.D. Williams, Science 283 (1999) 1148–1150.
[3] M. Albrecht, M. Luta, A.L. Spek, G. van Koten, Nature 406 (2000) 970–974.
[4] R. Owen, W. Lin, Acc. Chem. Res. 35 (2002) 511–522.
[5] E. Holder, B.M.W. Langeveld, U.S. Schubert, Adv. Mater. 17 (2005) 1109–1121.
[6] D.M. Shin, I.S. Lee, Y.A. Lee, Y.K. Chung, Inorg. Chem. 42 (2003) 2977–2982.
[7] M.A. Withersby, A.J. Blake, N.R. Champness, P.A. Cooke, P. Hubberstey, W.S. Li, M. Schröder, Inorg. Chem. 38 (1999) 2259–2266.
[8] D.M. Shin, I.S. Lee, Y.K. Chung, M.S. Lah, Inorg. Chem. 42 (2003) 5459–5461.
[9] K. Mitsurs, M. Shimamura, S.I. Noro, S. Minakoshi, A. Asami, K. Seki, S. Kitagawa, Chem. Mater. 12 (2000) 1288–1299.
[10] M. Eddaoudi, J. Kim, N. Rosi, D. Vodak, J. Wachter, M. O'Keeffe, O.M. Yaghi, Science 295 (2002) 469–472.
[11] C.D. Wu, C.Z. Lu, H.H. Zhuang, J.S. Huang, J. Am. Chem. Soc. 124 (2002) 3836–3837.
[12] M. Padmanabhan, K.C. Joseph, A. Thirumurugan, X.Y. Huang, T.J. Emge, J. Li, Inorga, Chim. Acta 360 (2007) 2583–2588.
[13] X. Yin, J. Tao, R.B. Huang, L.S. Zheng, Main Group Met. Chem. (2002) 691.
[14] J.H. Luo, M.C. Hong, R.H. Wang, R. Cao, L. Han, D.Q. Yuan, Z.Z. Lin, Y.F. Zhou, Inorg. Chem. 42 (2003) 4486–4488.
[15] J. Tao, X. Yin, Y.B. Jiang, L.F. Yang, R.B. Huang, L.S. Zheng, Eur. J. Inorg. Chem. (2003) 2678–2682.
[16] X.J. Li, R. Cao, W.H. Bi, Y.Q. Wang, Y.L. Wang, X. Li, Z.G. Guo, Cryst. Growth Des. 5 (2005) 1651–1656.
[17] Y.X. Ren, S.P. Chen, S.L. Gao, J. Coord. Chem. 59 (2006) 2135–2142.
[18] G. Xie, Q.Z. Shi, Inorg. Chim. Acta 359 (2006) 2047–2052.
[19] D.L. Long, R.J. Hill, A.L. Blake, N.R. Champness, P. Hubberstey, D.M. Proserpio, C. Wilson, M. Schröder, Angew. Chem. Int. Ed. 43 (2004) 1851–1853.
[20] Y.P. Ren, L.S. Long, B.W. Mao, Y.Z. Yuan, R.B. Huang, L.S. Zheng, Angew. Chem. Int. Ed. 42 (2003) 532–534.
[21] W.S. Liu, T.Q. Jiao, Y.Z. Li, Q.Z. Liu, M.Y. Tan, H. Wang, L.F. Wang, J. Am. Chem. Soc. 126 (2004) 2280–2281.
[22] G. Mancino, A.J. Ferguson, A. Beeby, N.J. Long, T.S. Jones, J. Am. Chem. Soc. 127 (2005) 524–525.
[23] S.K. Ghosh, P.K. Bharadwaj, Inorg. Chem. 44 (2005) 3156–3161.
[24] Y.G. Huang, B.L. Wu, D.Q. Yuan, Y.Q. Xu, F.L. Jiang, M.C. Hong, Inorg. Chem. 46 (2007) 1171–1176.
[25] F. Luo, Y.X. Che, J.M. Zheng, Cryst. Growth Des. 6 (2006) 2432–2434.
[26] D.L. Long, A.J. Blake, N.R. Champness, M. Schoder, Chem. Commun. (2000) 1369–1370.
[27] Y.C. Liang, R. Cao, W.P. Su, M.C. Hong, W.J. Zhang, Angew. Chem. Int. Ed. 39 (2000) 3304–3307.
[28] P.K. Chen, Y.X. Che, J.M. Zheng, Inorg. Chem. Commun. 10 (2007) 187–190.
[29] W. Zhao, J. Fan, T. Okamura, W.Y. Sun, N. Ueyama, Microporous Mesoporous Mat. 78 (2005) 265–279.
[30] D.T. Lill, A.B. Dias, C.L. Cahill, Inorg. Chem. 46 (2007) 3960–3965.
[31] J.J. Wang, L. Gou, H.M. Hu, Z.X. Han, D.S. Li, G.L. Xue, M.L. Yang, Q.Z. Shi, Cryst. Growth Des. 7 (2007) 1514–1521.
[32] G.M. Sheldrick, SHELXS 97, Program for Crystal Structure Solution, University of Göttingen, Göttingen, 1997.
[33] M.E. Davis, R.F. Lobo, Chem. Mater. 4 (1992) 756–768.
[34] G. Blasse, B.C. Grabmaier, Luminescent Materials, Springer, New York, 1994.
[35] S.I. Weissman, J. Chem. Phys. 10 (1942) 214–217.
[36] N. Sabbatini, M. Guardigli, J.M. Lehn, Coord. Chem. Rev. 123 (1993) 201–228.
[37] F. Gutierrez, C. Tedeschi, L. Maron, J.P. Daudey, R. Poteau, J. Azema, P. Tisnes, C. Picard, Dalton Trans. (2004) 1334–1347.
[38] M.D. Regulacio, M.H. Pablico, J.A. Vasquez, P.N. Myers, S. Gentry, M. Prushan, S.W. Tam-Chang, S.L. Stoll, Inorg. Chem. 47 (2006) 1512–1523.
[39] S. Sato, M. Wada, Bull. Chem. Soc. Jpn. 43 (1970) 1955–1962.
[40] S.L. Wu, Y.L. Wu, Y.S. Yang, J. Alloys Comp. 180 (1994) 399–403.

[41] D.L. Dexter, J. Chem. Phys. 21 (1953) 836–839.
[42] T.D. Brown, T.M. Shepherd, J. Chem. Soc. Dalton Trans. (1973) 336–340.
[43] Y.S. Song, B. Yan, Z.X. Chen, J. Mol. Struct. 750 (2005) 101–108.
[44] Y.S. Song, B. Yan, Z.X. Chen, J. Solid State Chem. 177 (2004) 3805–3814.
[45] K.Z. Tang, J. Zhang, Y. Tang, W.S. Liu, M.Y. Tan, Y.X. Sun, Inorg. Chim. Acta 359 (2006) 1207–1214.
[46] O.L. Malta, M.A. Couto dos Santos, L.C. Thompson, N.K. Ito, J. Lumin. 69 (1996) 77–84.
[47] E.E.S. Teotonio, J.G.P. Espinola, H.F. Brito, O.L. Malta, S.F. Oliveria, D.L.A. de Foria, C.M.S. Izumi, Polyhedron 21 (2002) 1837–1844.
[48] M. Xiao, P.R. Selvin, J. Am. Chem. Soc. 123 (2001) 7067–7073.
[49] W. De, W. Horrocks, D.R. Sudnick, J. Am. Chem. Soc. 101 (1979) 334–340.